

PCCP

Accepted Manuscript



This is an *Accepted Manuscript*, which has been through the Royal Society of Chemistry peer review process and has been accepted for publication.

Accepted Manuscripts are published online shortly after acceptance, before technical editing, formatting and proof reading. Using this free service, authors can make their results available to the community, in citable form, before we publish the edited article. We will replace this *Accepted Manuscript* with the edited and formatted *Advance Article* as soon as it is available.

You can find more information about *Accepted Manuscripts* in the [Information for Authors](#).

Please note that technical editing may introduce minor changes to the text and/or graphics, which may alter content. The journal's standard [Terms & Conditions](#) and the [Ethical guidelines](#) still apply. In no event shall the Royal Society of Chemistry be held responsible for any errors or omissions in this *Accepted Manuscript* or any consequences arising from the use of any information it contains.

Phase transitions in free water nanoparticles. Theoretical modeling of $[\text{H}_2\text{O}]_{48}$ and $[\text{H}_2\text{O}]_{118}^\dagger$

Aleš Vítek ^{*a} and René Kalus ^{b‡}

Received Xth XXXXXXXXXXXX 20XX, Accepted Xth XXXXXXXXXXXX 20XX

First published on the web Xth XXXXXXXXXXXX 200X

DOI: 10.1039/b000000x

Classical parallel-tempering Monte Carlo simulations of $[\text{H}_2\text{O}]_{48}$ and $[\text{H}_2\text{O}]_{118}$ have been performed in the isothermal-isobaric ensemble and a two-dimensional multiple-histogram method has been used to calculate the heat capacity of the two clusters. A semiempirical procedure is proposed for the inclusion of quantum effects and transformed heat capacity profiles are compared with state-of-the-art experimental data [Phys. Rev. Lett. 103 (2009) 073401, C. Hock et al.] A very good agreement is achieved. A detailed analysis of the simulation data is provided to get an insight into the nature of the phase change which takes place in the two clusters at $T \approx 100$ K.

1 Introduction

Free water clusters and nanoparticles play an important role in many areas of physics and chemistry and have thus been a subject of numerous experimental and theoretical studies. Among others, a recent development in the measurement of their caloric curves^{1,2} has enabled detailed experimental investigations of their phase transitions, most importantly melting and freezing. For example, internal energies and heat capacities have been measured for gas-phase $[\text{H}_2\text{O}]_{48}^-$ and $[\text{H}_2\text{O}]_{118}^-$ ³ over a broad range of temperatures, supposedly including their solid-liquid transition. The two systems can be considered good representatives of corresponding neutral water clusters since the attached electron is assumed to only marginally influence their thermodynamics³. Similar experimental results for protonated and deprotonated water clusters are available also showing that the charge does not have a strong influence⁴.

Larger cluster sizes are nowadays achievable, on the other hand, for theoretical modelings which are, in fact, highly desirable since many questions remain open without an appropriate theoretical analysis. For example, as discussed in detail in Ref. 3, only the low-temperature part of the caloric

curves of the two clusters can be recorded experimentally due to a significant overlap of the solid-liquid transition with the monomer evaporation. As a consequence, it is not clear how the caloric curve will evolve at higher temperatures and whether the solid-liquid transition develops a maximum on the heat-capacity curve or just a jump as seen in the experiment.

Numerical modeling of water clusters basically encounters two serious difficulties. One, the convergence of simulations is rather slow due to the complicated topology of the potential energy surface (PES), in particular for larger cluster sizes, and, two, light water molecules require a quantum treatment of nuclear degrees of freedom. While there are sophisticated methods for solving the former issue, e.g., parallel-tempering methods^{5,6}, and recent development of computational resources allows the theory to move to nanoscale sizes if classical approach is used^{7–10}, the full quantum simulation is still practicable only for the smallest sizes of a few molecular monomers. As an intermediate step for overcoming this deficiency, we present here a two-step algorithm consisting of a classical simulation providing converged classical data and a subsequent semiempirical modeling leading to an effective inclusion of quantum nuclear effects. We illustrate this semiempirical approach on a specific case of the cluster heat capacity which is generally considered a sensitive indicator of phase transitions in gas-phase clusters.

The rest of the paper is organized as follows. First, a semiempirical scheme for the inclusion of quantum effects is discussed for the heat capacity in Sec. 2 and tested against a specific case of $[\text{H}_2\text{O}]_{10}$ for which a full quantum calculation is available¹¹. Then, the semiempirical approach is applied to $[\text{H}_2\text{O}]_{48}$ and $[\text{H}_2\text{O}]_{118}$ and the results are compared with recent experiments³ on $[\text{H}_2\text{O}]_{48}^-$ and $[\text{H}_2\text{O}]_{118}^-$. Comparison with other simulations on larger water clusters is also included for completeness. Finally, conclusive remarks are given in Sec. 4.

2 Semiempirical inclusion of quantum effects

The basic idea of the present approach consists in performing a transformation of the classical heat capacity curve, C_c , to get an estimate of the corresponding quantum (or experimental)

^a IT4Innovations National Supercomputing Center, VSB - Technical University of Ostrava, 17. listopadu 15, 708 33 Ostrava, Czech Republic. Fax: XX XXXX XXXX; Tel: +420597329656; E-mail: ales.vitek@vsb.cz

^b IT4Innovations National Supercomputing Center & Department of Applied Mathematics, VSB - Technical University of Ostrava, 17. listopadu 15, 708 33 Ostrava, Czech Republic.

heat capacity, C_q . The first step of this transformation is based on a known fact that classical simulations may well reproduce quantum results if the simulation temperature is increased to mimic quantum delocalization of nuclei^{12–14}. A first step on the way from classical to quantum heat capacity is thus as follows,

$$C_q^{(1)}(T) = C_c(\alpha T) \quad (1)$$

where $T_c = \alpha T$ and $\alpha > 1$. The second step then takes into account the fact that the harmonic approximation of the cluster PES is essentially exact at temperatures close to zero, $T \rightarrow 0$, and that the vibration part of the quantum heat capacity can thus be replaced, at low temperatures¹⁵, with the heat capacity calculated within the (quantum) harmonic approximation¹⁶,

$$C_q^{(\text{id})}(T) = \sum_{i=1}^{3N-6} k_B \varepsilon_i(T)^2 \frac{e^{\varepsilon_i(T)}}{[e^{\varepsilon_i(T)} - 1]^2}, \quad (2)$$

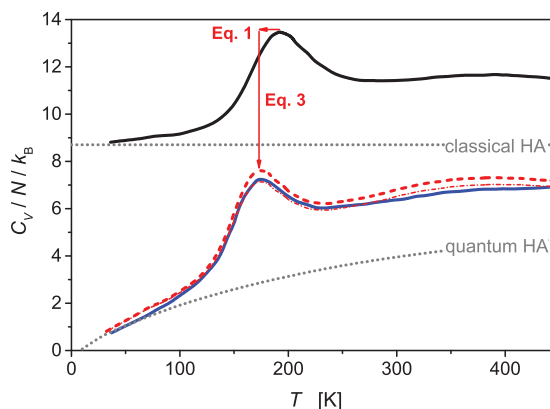
where $\varepsilon_i(T) = \hbar \omega_i / k_B T$, \hbar is the reduced Planck constant, k_B stands for the Boltzmann constant, N is the total number of atoms in the cluster, and ω_i represent cluster normal mode angular frequencies. However, the approximation $C_q(T) \approx C_q^{(\text{id})}(T)$ is valid only at temperatures well below the solid-liquid transition and, as the temperature increases, anharmonic corrections become important and have to be taken into account. In the present model, it is done via

$$C_q^{(2)}(T) = C_q^{(\text{id})}(T) + [C_c(\alpha T) - C_c^{(\text{id})}], \quad (3)$$

where $C_c^{(\text{id})} = (3N - 6)k_B$ is the vibration part of the classical heat capacity of the system calculated within the harmonic approximation. As a consequence, the anharmonic correction (the second term on the r.h.s. of Eq. 3) to the cluster heat capacity is taken into account at the classical level.

How the proposed semiempirical approach of Eq. 3 works is illustrated on a specific case of $[\text{H}_2\text{O}]_{10}$ in Fig. 1 for which both classical and quantum simulations were performed¹¹ under the same conditions. Similar results are obtained for another cluster, $[\text{H}_2\text{O}]_8$, for which both kinds of calculations were also reported in Ref. 11. Several observations are clear from Fig. 1. Firstly, a fairly good agreement is achieved between the full quantum treatment (lower full line) and the approximation of Eq. 3 (dashed line). A small shift to higher values seen for Eq. 3 with respect to the quantum curve may indicate that the anharmonic contribution to the heat capacity calculated at the classical level slightly overestimates the quantum one. Secondly, the quantum harmonic approximation (lower dotted curve) reproduces the full quantum simulation very well up to rather high temperatures ($T \approx 90$ K) even though only the most stable isomer of $[\text{H}_2\text{O}]_{10}$ has been considered in frequency calculations. Thirdly, note that a quantitative agreement is easily achieved between full quantum and

Fig. 1 Heat capacity of $[\text{H}_2\text{O}]_{10}$ per water molecule: upper full line – classical simulation of Ref. 11, lower full line (blue online) – quantum simulation of Ref. 11, thick dashed line (red online) – $C_q^{(2)}$ of Eq. 3 obtained for $\alpha = 1.12$, thin dash-dotted line (red online) – $C_q^{(2)}$ calculated via modified Eq. 4 with $\beta = 0.9$, gray dotted lines – heat capacity calculated within the harmonic approximation (HA). Arrows indicate the transformation of the classical simulation data via Eqs. 1 and 3.



semiempirical data if a phenomenological correction factor, β , is introduced in Eq. 3,

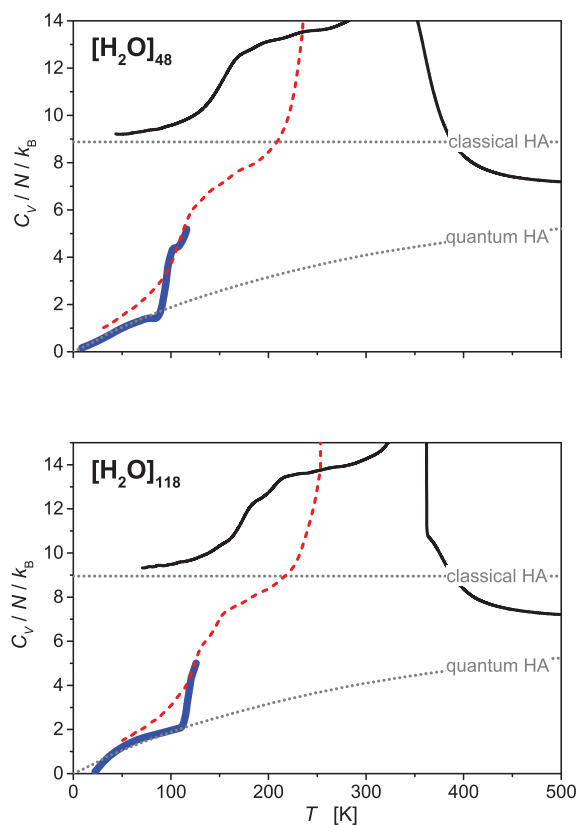
$$C_q^{(2)}(T) = C_q^{(\text{id})}(T) + \beta [C_c(\alpha T) - C_c^{(\text{id})}]. \quad (4)$$

Note also that the good correspondence is achieved over a broad range of temperatures even if the correction factor is assumed temperature-independent ($\beta \approx 0.9$). However, if a bit more phenomenology is introduced and an optimal $\beta(T)$ dependence is derived for $[\text{H}_2\text{O}]_{10}$ so that the full quantum heat capacity is reproduced with minimum residual, one gets an almost constant $\beta \approx 0.9$ only for $150 \text{ K} \leq T \leq 450 \text{ K}$ while a decrease to zero is observed for $T < 150 \text{ K}$. Such a behavior may mean that the anharmonic effects are gradually switched off at low temperatures.

3 Application to $[\text{H}_2\text{O}]_{48}$ and $[\text{H}_2\text{O}]_{118}$

The methodology described above has been applied to specific cases of $[\text{H}_2\text{O}]_{48}$ and $[\text{H}_2\text{O}]_{118}$ to analyze how experimental data³ can be reproduced by theory in this size range. As already mentioned, we believe that the calculations on neutral clusters can reproduce the experimental data obtained for cluster anions since the attached electron is believed to have only a negligible effect on the phase behavior of the two clusters³. The results are summarized in Fig. 2 where heat capacities are displayed for both purely classical Monte Carlo simulations and subsequent transformation via Eq. 3, and compared with experimental curves.

Fig. 2 Heat capacity of $[\text{H}_2\text{O}]_{48}$ and $[\text{H}_2\text{O}]_{118}$ per water molecule: upper full line – classical simulation, dashed line (red online) – $C_q^{(2)}$ of Eq. 3 obtained for $\alpha = 1.40$, lower full line (blue online) – experimental data³. Dotted lines correspond to the heat capacity obtained at the harmonic approximation (HA) level.

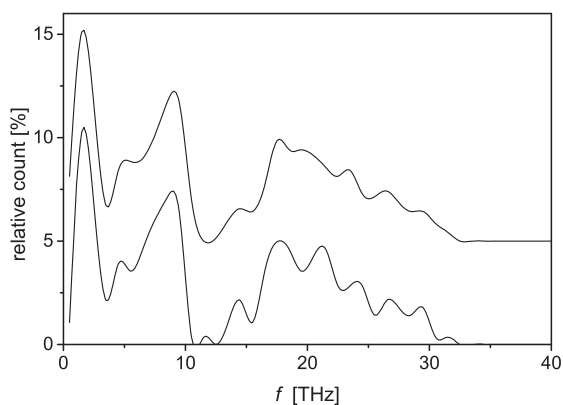


The classical Monte Carlo simulations have been performed in the isothermal-isobaric ensemble¹⁷, with pressure represented by a spherical hard-wall container of variable radius¹⁸ to prevent monomer evaporation, and combined with the two-dimensional multiple-histogram method^{18,19} as described recently in detail in Ref. 20. Parallel-tempering¹⁷, both along the temperature axis as well as along the pressure axis, has been used to accelerate the convergence of the simulation. Totally, 23 temperatures spanning an interval of $T \in [30, 1000]$ K and five pressures between $P = 10^5$ Pa and $P = 10^9$ Pa have been simulated in parallel and mixed periodically. The exceedingly large higher limit of the temperature and high pressures have been used for convergence purposes. Since the primary interest of the present study is on free nanoparticles, only the results obtained for the lowest pressure, $P = 10^5$ Pa, are considered here²¹. Totally, $2 \cdot 10^8$ MC steps²² have been generated for $[\text{H}_2\text{O}]_{48}$ and $4 \cdot 10^7$ for $[\text{H}_2\text{O}]_{118}$, one half of them being rejected at the beginning of each calculation to

reach thermal equilibrium. Only every 50th step has been included in gathering the energy-volume histograms needed for the two-dimensional density of states calculation to avoid non-physical correlations. A simple flexible TIP4P potential²³ has been used to represent the intermolecular interactions in water to keep the computational demands reasonable.

Another input to Eq. 3, namely the harmonic-approximation heat capacity ($C_q^{(id)}$), has been calculated as follows. First, a representative set of 240 configurations has been picked up from the $T = 30$ K (and $P = 10^5$ Pa) calculation and optimized locally. Second, the normal mode frequencies of the optimized structures have been calculated and used in Eq. 2 to obtain corresponding heat capacities. Finally, the heat capacities calculated for all the recorded structures have been averaged. It is noteworthy, however, that almost identical $C_q^{(id)}$ curves have been obtained for different equilibrium structures and, as a consequence, all of them closely coincide with the averaged curves given in Fig. 2. Intermolecular vibration spectra of the lowest energy isomers occurring in Monte Carlo simulations are depicted for both sizes in Fig. 3. Note that a close similarity to the spectra calculated recently by Chen and Hansen¹⁵ can be seen if Fig. 3 is compared with Fig. 4 of Ref. 15.

Fig. 3 Intermolecular vibration spectra of water clusters. Spectra are calculated in harmonic approximations and normalized according the number of the intermolecular vibration models. The bottom line corresponds to $[\text{H}_2\text{O}]_{48}$, the upper line represents the spectrum of $[\text{H}_2\text{O}]_{118}$ and is shifted by 5% upwards.



Several observations are clear from Fig. 2. Firstly, the curves calculated within the harmonic approximation agree very well with the recorded experimental points up to rather high temperatures ($T \approx 90$ K for $[\text{H}_2\text{O}]_{48}$ and $T \approx 110$ K for $[\text{H}_2\text{O}]_{118}$). This compares well with an observation of Ref. 3 that the $[\text{H}_2\text{O}]_{48}$ and $[\text{H}_2\text{O}]_{118}$ caloric curves agree well with the curve recorded for bulk ice. It is surprising, however, that a simple TIP4P potential can reproduce the normal

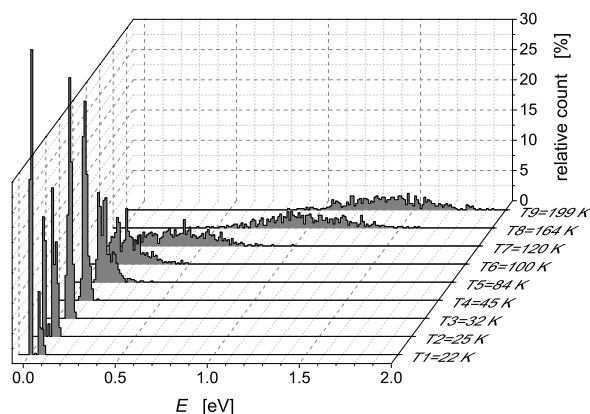
mode vibrations of both clusters with such an accuracy. A more detailed analysis further reveals that only low-frequency inter-molecular vibrations (up to $f \approx 7 - 10$ THz) contribute. On the average, about 35 – 50% of inter-molecular vibration modes are active while the remaining inter-molecular vibrations ($f \approx 13 - 32$ THz) and all the intra-molecular vibrations are effectively frozen. Secondly, the curves obtained from classical calculations and subsequently processed by Eq. 3 also agree fairly well with the experiment, minor discrepancies may mostly be attributed to the simple interaction model employed in our calculations. Only the differences seen at the start of the rise of the heat capacity (indicating the onset of the solid-liquid transition) may be an artifact of Eq. 3. As already discussed for $[\text{H}_2\text{O}]_{10}$, this is probably due to the fact that the classical anharmonic correction included in Eq. 3 overestimates the true one, particularly at low temperatures. Indeed, if Eq. 4 is used instead and $\beta(T)$ is adjusted to best reproduce the experimental points, one gets β close to 1 for $T \geq 100$ K, but dropping sharply to zero at lower temperatures. The anharmonic effects are thus highly probably heavily damped at low temperatures, as already observed for $[\text{H}_2\text{O}]_{10}$, for the larger cluster sizes as well.

An important question unresolved in Ref. 3 is whether the step on the heat capacity curves of $[\text{H}_2\text{O}]_{48}^-$ and $[\text{H}_2\text{O}]_{118}^-$ recorded experimentally in the transition region is a left wing of a maximum or if the transition is accompanied only by the observed stepwise rise. According to our calculations, the latter is the case. No peak develops in the heat capacity profile of either $[\text{H}_2\text{O}]_{48}$ or $[\text{H}_2\text{O}]_{118}$ across the transition region, just a steep rise followed by another, much slower increase up to the boiling region. This observation agrees well with Ref. 9 from which it follows that a maximum on the $[\text{H}_2\text{O}]_N$ heat-capacity curve is observed for the TIP4P potential only for small cluster sizes while this maximum completely flattens at $N \approx 20$ (cf. Fig. 13 of Ref. 9).

To see what structural transformations take place during the transition, we recorded, for selected temperatures, 480 randomly chosen configurations of $[\text{H}_2\text{O}]_{48}$, optimized them locally, and investigated their classical equilibrium energies and structures to see how different structural isomers enter the game as the phase transformation proceeds²⁴. Results are summarized in Fig. 4.²⁵ The temperatures considered in this figure cover the regions where (a) the cluster is solid (temperatures $T_1 - T_4$), (b) the first steep increase is observed in the heat capacity in simulations ($T_5 - T_7$), and where (c) a much slower rise of the heat capacity is observed (T_8 and T_9) prior to the onset of cluster boiling.

A clear message of Fig. 4 is that, in the solid region (temperatures $T_1 - T_4$), two families of energetically close isomers are populated. The difference between the binding energy of the isomers of the lower family and the lowest value recorded in our simulations is at maximum 0.02 eV (or

Fig. 4 Histograms of equilibrium energies of isomers of $[\text{H}_2\text{O}]_{48}$ detected at various temperatures of the solid-liquid transition region. The zero of energy corresponds to the most stable isomer of $[\text{H}_2\text{O}]_{48}$ detected in the calculation. Note that the temperatures shown on the right have been scaled using Eq. 1, $T = T_{\text{class}}/\alpha$ with $\alpha = 1.40$, where T_{class} is the temperature of corresponding classical simulation.



less than 0.5 meV per molecule) and about 0.12 eV (less than 3 meV per molecule) for the upper family. Isomers from the two families are quite similar to each other: they have approximately a spherical shape with the surface covered by tetragons, pentagons and hexagons; but, the lower energy isomers contain six water molecules inside while the higher energy ones have five inside molecules. Note that this is in good agreement with the structures reported recently for $[\text{H}_2\text{O}]_{N \leq 55}$ for the TTM2.1F potential²⁶ by Kazachenko and Thakkar²⁷; small differences in clusters geometry are probably due to different interaction models used in Ref. 27 and here.

The abundance of the lower-family isomers, however, decreases rapidly with increasing temperature from about 80% at $T_1 = 20$ K to 40% at $T_2 = 23$ K and, finally, to zero at $T \geq T_3 = 28$ K. At the beginning of (T_5) and along the steep rise of the heat capacity (T_6 and T_7), the abundance of the solid isomers decreases to zero and new structures, much higher in energy and much more disordered, emerge. Beyond the step in the heat capacity ($T \geq T_7$), no solid isomers are populated any longer and only disordered structures appear with a broad distribution of binding energies the maximum of which gradually moves to higher energies as the temperature increases. The cluster is liquid in this region and, as it heats up, more and more disordered and energetically richer parts of its configuration space are visited.

As mentioned in Ref. 3, the liquid region overlaps significantly with the evaporative region. As follows from our calculations, the cluster, if kept at normal pressure, $P = 10^5$ Pa, starts to boil at $T \approx 200$ K, which is indicated by a sharp and high maximum on the cluster heat capacity curve slightly

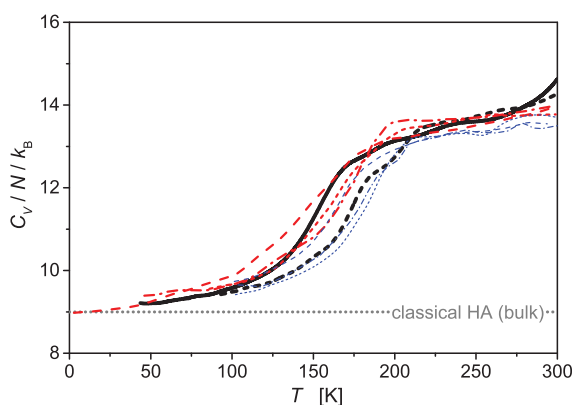
above this temperature ($T \approx 250$ K) (see Fig. 2).

Following the recommendation of one of the referees, in Fig. 5, we compare selected results of simulations on larger TIP4P water clusters as reported in the literature with the classical heat capacities calculated in this work. In particular, heat capacity curves obtained^{9,10} for $N = 30, 50$ and 100 via the Wang-Landau sampling approach^{28,29} are considered together with micro-canonical (NVE) Monte Carlo data⁸ for $N = 40, 60$ and 80 to cover the span of cluster sizes considered in this work. General conclusions, clear from Fig. 5, may be as follows: a) data corresponding to different cluster sizes ($N = 30 - 118$) and computational approaches (Wang-Landau, NVE and NPT Monte Carlo) correspond very well to each other qualitatively and even quantitative differences are not dramatic, b) similarly, the use of different TIP4P potentials (rigid vs. flexible) does also not have a major effect, and, finally, c) for all the clusters considered in Fig. 5, the (solid-liquid) phase change is accompanied by a more or less steep rise of the cluster heat capacity occurring at transition temperatures (around $T \approx 170$ K) and followed by a plateau (instead of developing of a clear maximum) above $T \approx 200$ K. In addition, quite interestingly, even though the solid-liquid transition of the water clusters of sizes $N \approx 30 - 120$ is still very different from the melting of bulk TIP4P ices, for which, e.g., $T_{\text{melt}} \approx 230 - 270$ K (see Table I of Ref. 30), qualitatively similar and quantitatively rather close features, almost independent on the cluster size, are seen on the respective heat capacity profiles.

4 Conclusions

In summary, classical parallel-tempering Monte Carlo⁶ calculations have been performed for $[\text{H}_2\text{O}]_{48}$ and $[\text{H}_2\text{O}]_{118}$ in the isothermal-isobaric ensemble¹⁷. Two-dimensional multiple-histogram method¹⁸⁻²⁰ has been used to calculate the heat capacity of both clusters at low pressure and over a broad range of temperatures. Simple semiempirical procedure has been proposed for including quantum nuclear effects in the caloric curve and the transformed heat capacity curves have been compared with recent experimental data³. A very good agreement has been achieved. In addition, it has been found that the quantum harmonic approximation reproduces the experimental heat capacities of both clusters very well up to rather high temperatures ($T \approx 100$ K). The analysis of isomers populated at various temperatures clearly shows that a transition from ordered (solid-like) phase to disordered (liquid-like) phase takes place at temperatures at which a steep rise of the heat capacity has been detected. This transition is not accompanied by any maximum on the heat capacity curve. A comparison with previous classical simulations on TIP4P water clusters⁸⁻¹⁰ shows a good correspondence between our data and literature data as well as a quite surprising fact that, for $[\text{H}_2\text{O}]_{N \approx 30-120}$, their

Fig. 5 The heat capacity of selected $[\text{H}_2\text{O}]_N$ clusters as obtained from classical simulations using TIP4P interaction potentials: thick curves (black on-line): the present calculations for $[\text{H}_2\text{O}]_{48}$ (solid) and $[\text{H}_2\text{O}]_{118}$ (dashed); semi-thick curves (red on-line): Wang-Landau sampling calculations on $N = 30$ (dashed)⁹, $N = 50$ (dot-dashed)¹⁰, and $N = 100$ (short-dashed)⁹; thin curves (blue on-line): micro-canonical Monte Carlo calculations⁸ on $N = 40$ (dashed), $N = 60$ (dot-dashed), and $N = 80$ (short-dashed). Note that a value of $3k_B$ has been added to the literature data (calculated for rigid TIP4P potentials) to include the intra-molecular vibration contribution.



melting behavior is only slightly dependent on the cluster size, variant of the TIP4P potential used, and simulation approach.

Acknowledgments

This work has been financially supported by EU Operational Programmes *Research and Development for Innovations* and *Education for Competitiveness* funded by Structural Funds of the European Union and the state budget of the Czech Republic (grants CZ.1.05/1.1.00/02.0070 and CZ.1.07/2.3.00/30.0055), and by the Ministry of Education of the Czech Republic (grants LM2011033 and 7E12028). The calculations were performed on the HPC resources of the University of Oslo, Norway, made available via DECI/PRACE-2IP funded from the EU 7th Framework Programme (grant RI-283493), and on the computers of the IT4Innovations National Supercomputing Center, VSB-TU of Ostrava (grant IT4I-3-3).

References

- 1 M. Schmidt, R. Kusche, W. Kronmüller, B. von Issendorff and H. Haberland, *Phys. Rev. Lett.*, 1997, **79**, 99–102.
- 2 M. Schmidt, R. Kusche, B. von Issendorff and H. Haberland, *Nature*, 1998, **393**, 238–240.
- 3 C. Hock, M. Schmidt, R. Kuhn, C. Bartels, L. Ma, H. Haberland and B. von Issendorff, *Phys. Rev. Lett.*, 2009, **103**, 073401.

- 4 J. Boulon, I. Braud, S. Zamith, P. Labastie and J.-M. L'Hermite, *J. Chem. Phys.*, 2014, **140**, 164305.
- 5 C. J. Geyer, *Computing Science and Statistics: Proceedings of the 23rd Symposium on the Interface*, American Statistical Association, New York, 1991, p. 156.
- 6 C. J. Geyer and E. A. Thompson, *J. Am. Stat. Assoc.*, 1995, **90**, 909.
- 7 J. Douady, F. Calvo and F. Spiegelman, *Eur. Phys. J. D*, 2009, **52**, 47.
- 8 J. Gelman-Constantin, M. A. Carignano, I. Szleifer, E. J. Marceca and H. R. Corti, *J. Chem. Phys.*, 2010, **133**, 024506.
- 9 J. Yin and D. P. Landau, *J. Chem. Phys.*, 2011, **134**, 074501.
- 10 J. Yin and D. P. Landau, *Comp. Phys. Commun.*, 2012, **183**, 1568–1573.
- 11 P. A. Frantsuzov and V. A. Mandelshtam, *J. Chem. Phys.*, 2008, **128**, 094304.
- 12 Ll. Uranga-Piña, A. Martínez-Mesa, J. Rubayo-Soneira and G. Rojas-Lorenzo, *Chem. Phys. Lett.*, 2006, **429**, 450–456.
- 13 Ll. Uranga-Piña, A. Martínez-Mesa, L. García-Reyes and J. Rubayo-Soneira, *Phys. Chem. Chem. Phys.*, 2009, **11**, 5358–5368.
- 14 R. Kalus, F. Karlický, B. Lepetit, I. Paidarová and F. X. Gadea, *J. Chem. Phys.*, 2013, **139**, 204310.
- 15 H. Chen and K. Hansen, *Chem. Phys. Lett.*, 2014, **610**, 369–374.
- 16 In the experiment, the vibration part of the cluster heat capacity is measured, so, we will not consider the translational and rotational contributions in this work.
- 17 T. Okabe, M. Kawata, Y. Okamoto and M. Mikami, *Chem. Phys. Lett.*, 2001, **335**, 435–439.
- 18 H. P. Cheng, X. Li, R. L. Whetten and R. S. Berry, *Phys. Rev. A*, 1992, **46**, 791–800.
- 19 A. Pal and S. K. Roy, *Phys. Rev. E*, 2004, **69**, 021709.
- 20 A. Vitek and R. Kalus, *Comp. Phys. Commun.*, 2014, **185**, 1595.
- 21 Note that the classical heat capacities depicted in Fig. 2 are the constant-pressure heat capacities. However, for condensed phases (solid and liquid) and for the low pressure considered ($P = 10^5$ Pa), the values are basically the same as we would get for the constant-volume heat capacity.
- 22 A step consists of successive translational, rotational and deformation displacements of all molecules in the cluster, and an attempt of configuration-volume exchange between two selected $P - T$ simulation runs.
- 23 M. A. Gonzalez and J. L. F. Abascal, *J. Chem. Phys.*, 2011, **135**, 224516.
- 24 F. H. Stillinger and T. A. Weber, *Phys. Rev. A*, 1982, **25**, 978–989.
- 25 Clearly, not all minima on the potential energy surface of $[\text{H}_2\text{O}]_{48}$ (or even $[\text{H}_2\text{O}]_{118}$) can effectively be sampled within a practicable simulation, simply because their number is too large for the cluster sizes considered and computational resources available. However, representative structures of various isomer families, and in particular their binding energies, will be highly probably sampled at some level of completeness and, as a consequence, the counts of various structural isomers represented by their energies are believed to be realistically modeled in these large clusters even if they are obtained from simulations which are "incomplete" in the above mentioned sense.
- 26 G. S. Fanourgakis, S. S. Xantheas and S. Sotiris, *J. Chem. Phys.*, 2008, **128**, 074506.
- 27 S. Kazachenko and A. J. Thakkar, *J. Chem. Phys.*, 2013, **138**, 194302.
- 28 F. G. Wang and D. P. Landau, *Phys. Rev. Lett.*, 2001, **86**, 2050.
- 29 F. G. Wang and D. P. Landau, *Phys. Rev. E*, 2001, **64**, 056101.
- 30 R. G. Fernández, J. L. F. Abascal and C. Vega, *J. Chem. Phys.*, 2006, **124**, 144506.